Electronic Supplementary Information (ESI)

Helical nanofibers of *N*-(perfluorooctanoyl)cysteine ethyl ester in its coordination polymers of Ag^+

Dan-Dan Tao,[a] Jin-Hong Wei,[a] Xiao-Sheng Yan,[a] Qian Wang,[a] Bo-Han Kou,[a] Na Chen[a] and Yun-Bao Jiang[a,*]

Department of Chemistry, College of Chemistry and Chemical Engineering, the MOE Key Laboratory of Spectrochemical Analysis and Instrumentation, and iChEM, Xiamen University, Xiamen 361005, China

E-mail: ybjiang@xmu.edu.cn

TABLE OF CONTENTS

S1. Experimental

S1.1 General

All chemicals and solvents purchased from Energy Chemical, except otherwise described, were used without further purification. ^{1}H NMR and ^{13}C NMR spectra were recorded using AVANCE III HD 500MHz in $CDCl_3$ with TMS. ^{19}F NMR spectra were recorded using Ascend 600 MHz in $CDCl_3$ with TMS. Absorption spectra were recorded on a Thermo Evolution 300 spectrophotometer. CD spectrometry was conducted using JASCO J-810 Circular Dichroism Chiroptical Spectrometer. Steady-state fluorescence measurements were conducted using a HITACHI F-4500 spectrofluorometer. HRMS (high-resolution MS) was recorded on Bruker Impact II.

S1.2 Synthesis

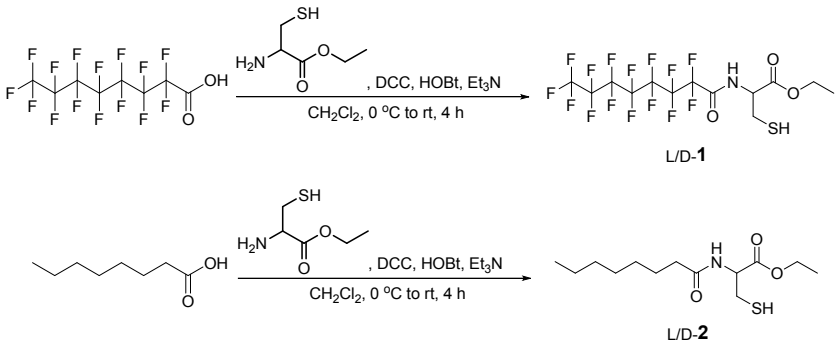

Scheme S1 Syntheses of L-**1**/D-**1** and L-**2**/D -**2**.

L-**1**/D-**1**: L-/D-cysteine ethyl ester (2 mmol), 1-hydroxybenzotriazole (2 mmol) and triethylamine (2 mmol) in CH_2Cl_2 (10 mL) were added pentadecafluorooctanoic acid (2 mmol). The mixture was stirred at 0 °C for 20 min, then dicyclohexylcarbodiimide (2 mmol) was added and stirred at room temperature for 4 h. After filtration and solvent evaporation, the crude product was purified by silica gel column chromatography, and white powder of L-**1**/D-**1** was obtained (0.46 g, 42% yield).

L-**1**/D-**2**: L-/D-cysteine ethyl ester (2 mmol), 1-hydroxybenzotriazole (2 mmol) and triethylamine (2 mmol) in CH_2Cl_2 (10 mL) were added octanoic acid (2 mmol). The mixture was stirred at 0 °C for 20 min, then dicyclohexylcarbodiimide (2 mmol) was added and stirred at room temperature for 4 h. After filtration and solvent evaporation, the crude product was purified by silica gel column chromatography, and light yellow powder of L-**2**/D-**2** was obtained (0.21g, 60% yield).

L-**1**: **^{1}H NMR** (500 MHz, $CDCl_3$) δ/ppm 7.28 (d, J = 6.3 Hz, 1H), 4.89–4.86 (m, 1H), 4.33–4.29 (m, 2H), 3.12–3.07 (m, 2H), 1.35 (t, J = 9.0 Hz 1H), 1.33 (t, J = 7.1 Hz, 3H); **^{13}C NMR** (126 MHz, $CDCl_3$) δ/ppm 168.43, 157.25, 117.12, 110.82, 110.65, 110.46, 110.19, 108.87, 108.37, 62.82, 54.09, 26.00, 14.12; **HRMS** (ESI^+) $[M+Na]^+$: calcd for $C_{13}H_{10}F_{15}NO_3SNa$ 568.0040, found 568.0038.

D-**1**: **^{1}H NMR** (500 MHz, $CDCl_3$) δ/ppm 7.29 (d, J = 5.6 Hz, 1H), 4.89–4.86 (m, 1H), 4.36–4.26 (m, 2H), 3.15–3.05 (m, 2H), 1.34 (t, J = 9.0 Hz, 1H), 1.33 (t, J = 7.1 Hz, 3H); **^{13}C NMR** (126 MHz, $CDCl_3$) δ/ppm 168.42, 157.27, 117.12, 110.82, 110.65, 110.47, 110.20, 108.87, 108.38, 62.80, 54.08, 25.99, 14.11; **HRMS** (ESI^+) $[M+Na]^+$: calcd for $C_{13}H_{10}F_{15}NO_3SNa$ 568.0040, found 568.0043.

L-**2**: **^{1}H NMR** (500 MHz, $CDCl_3$) **：** δ/ppm 6.34 (d, J = 6.5 Hz, 1H), 4.88–4.85 (m, 1H), 4.30–4.20 (m, 2H), 3.03–3.00 (m, 2H), 2.25 (t, J = 7.7 Hz, 2H), 1.67–1.61 (m, 2H), 1.32–1.27 (m, 12H), 0.87 (t, J = 7.1 Hz, 3H); **^{13}C NMR** (126 MHz, $CDCl_3$) δ/ppm 172.91, 170.20, 61.98, 53.38, 36.56, 31.65, 29.18, 28.96, 26.93, 25.59, 22.58, 14.19, 14.02; **HRMS** (ESI^+) $[M+Na]^+$: calcd for $C_{13}H_{25}NO_3SNa$ 298.1453, found 298.1448.

D-**2**: **^{1}H NMR** (500 MHz, $CDCl_3$) δ/ppm 6.34 (d, J = 6.6 Hz, 1H), 4.88–4.85 (m, 1H), 4.28–4.21 (m, 2H), 3.03–3.00 (m, 2H), 2.26 (t, J = 7.5 Hz, 2H), 1.68–1.62 (m, 2H), 1.32–1.27 (m, 12H), 0.87 (t, J = 7.1 Hz, 3H); **^{13}C NMR** (126 MHz, $CDCl_3$) δ/ppm 172.89, 170.20, 61.98, 53.37, 36.57, 31.66, 29.18, 28.96, 26.93, 25.59, 22.58, 14.19, 14.02; **HRMS** (ESI^+) $[M+Na]^+$: calcd for $C_{13}H_{25}NO_3SNa$ 298.1453, found 298.1448.

S1.3 References

1. T. Terauchi, S. Machida and S. Komba, *Tetrahedron Lett.*, 2010, **51**, 1497.

2. M. Brindisi, S. Butini, S. Franceschini, S. Brogi, F. Trotta, S. Ros, A. Cagnotto, M. Salmona, A. Casagni, M. Andreassi, S. Saponara, B. Gorelli, P. Weikop, J. D. Mikkelsen, J. Scheel-Kruger, K. Sandager-Nielsen, E. Novellino, G. Campiani and S. Gemma, *J. Med. Chem*., 2014, **57**, 9578.

S2. Additional data

S2.1 Experimental data

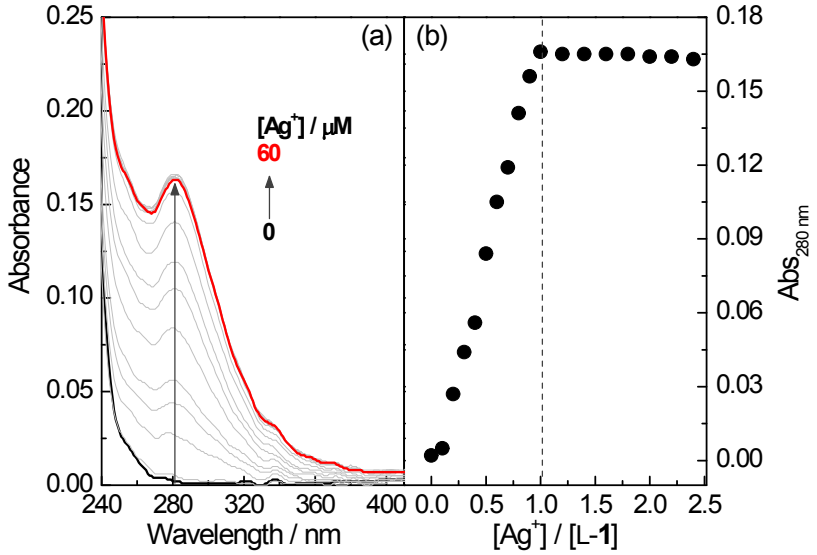

Fig. S1 (a) Absorption spectra of L-**1** in EtOH in the presence of Ag^+ and (b) plots of absorbance at 280 nm against concentration of Ag^+. [L-**1**] = 25 μM.

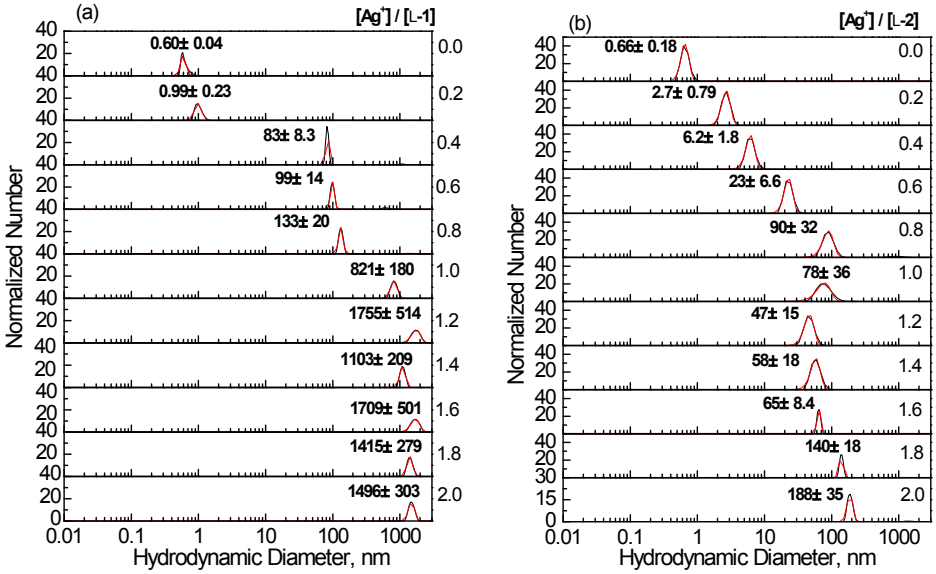

Fig. S2 Hydrodynamic diameters of L-**1** (a) and L-**2** (b) in EtOH in the presence of Ag^+ of increasing concentration. [L-**1**] = [L-**2**] = 25 μM.

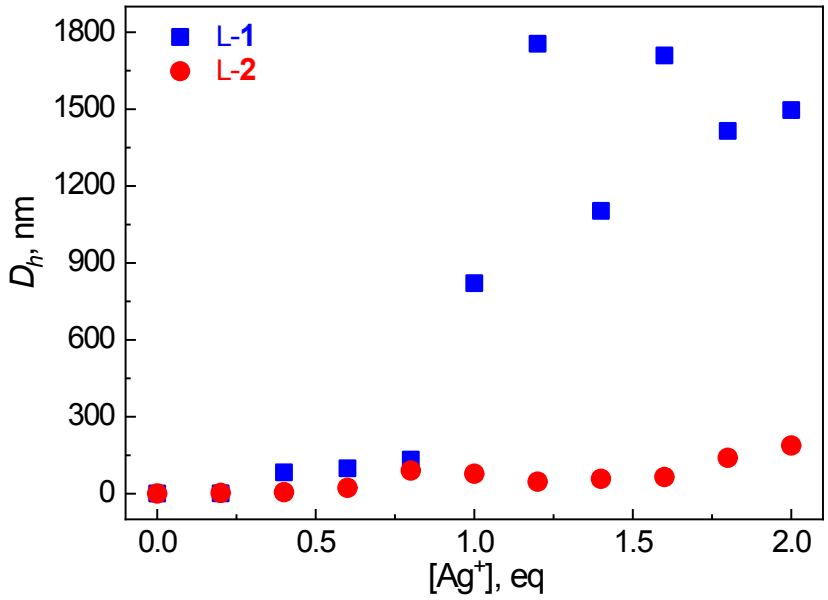

Fig. S3 Hydrodynamic diameters of L-**1** (a) and L-**2** (b) in EtOH in the presence of Ag^+ of increasing concentration. [L-**1**] = [L-**2**] = 25 μM.

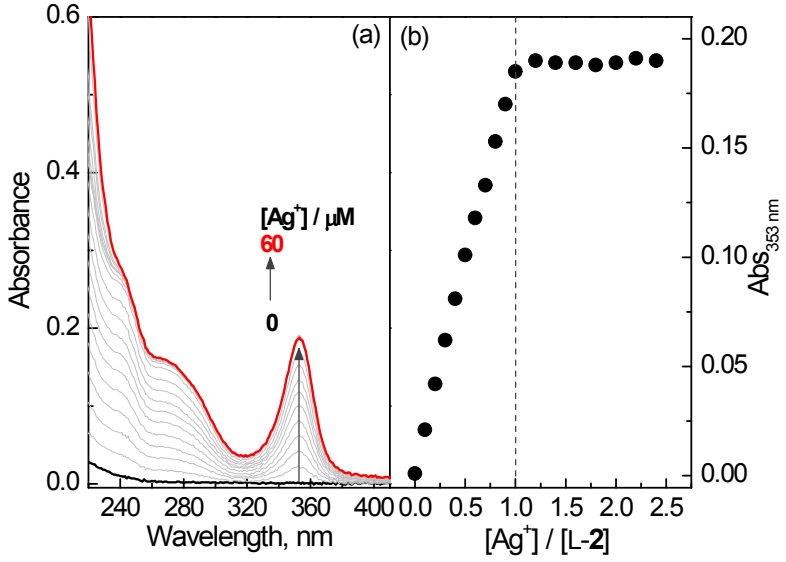

Fig. S4 (a) Absorption spectra of L-**2** in EtOH in the presence of Ag^+ and (b) plots of absorbance at 353 nm against concentration of Ag^+. [L-**2**] = 25 μM.

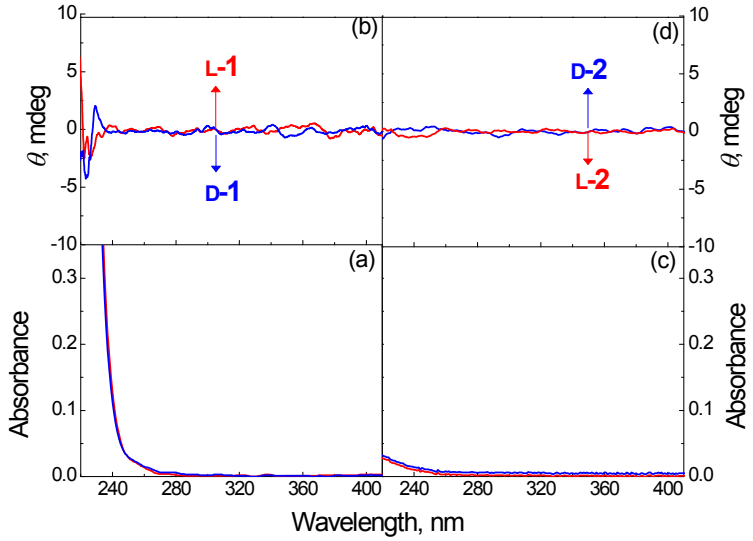

Fig. S5 Absorption and CD spectra of L-**1**/D-**1** (a, b) and L-**2**/D-**2** (c, d) in EtOH. [L-**1**] = [D-**1**] = [L-**2**] = [D-**2**] = 25 μM.

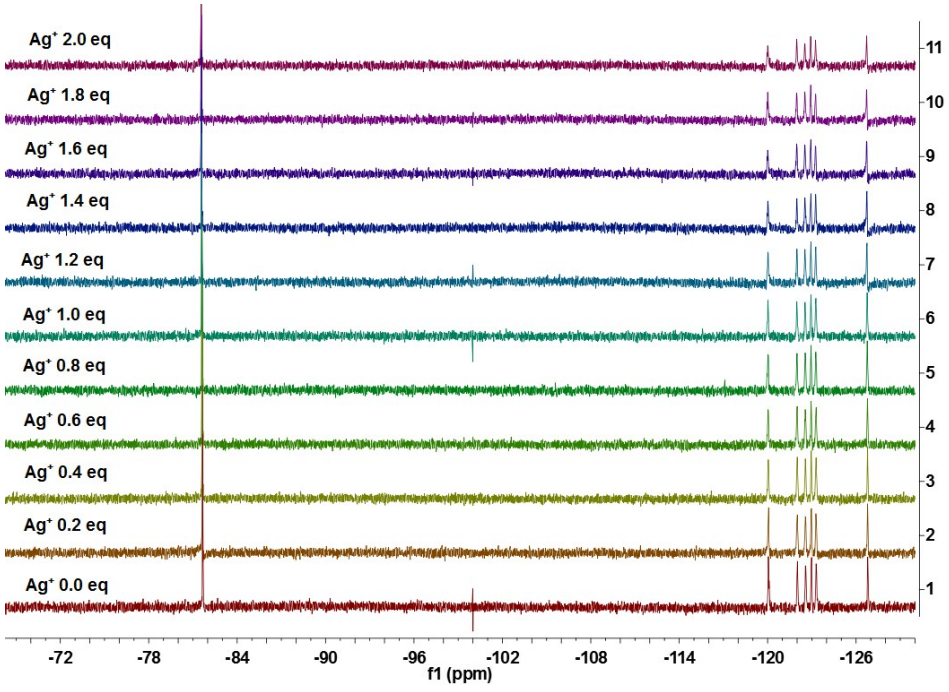

Fig. S6 ^{19}F NMR titrations of L-**1** by Ag^+ in EtOD. [L-**1**] = 50 μM.

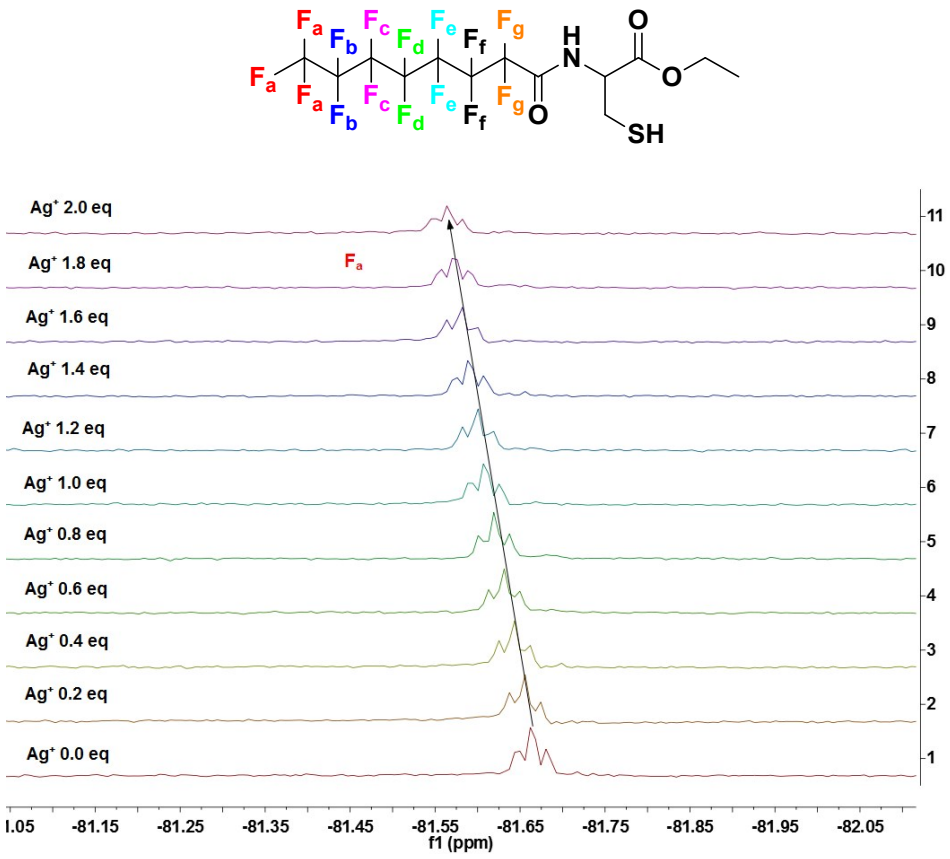

Fig. S7 Partial ^{19}F NMR spectra of F_a of L-**1** in the presence of Ag^+ in EtOD. [L-**1**] = 50 μM.

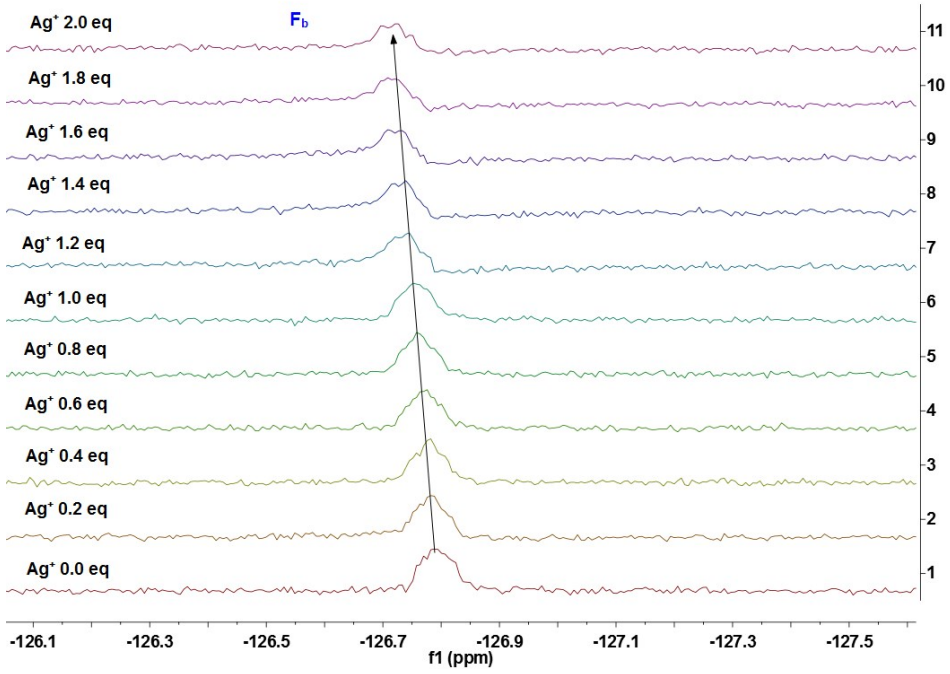

Fig. S8 Partial ^{19}F NMR spectra of F_b of L-**1** in the presence of Ag^+ in EtOD. [L-**1**] = 50 μM.

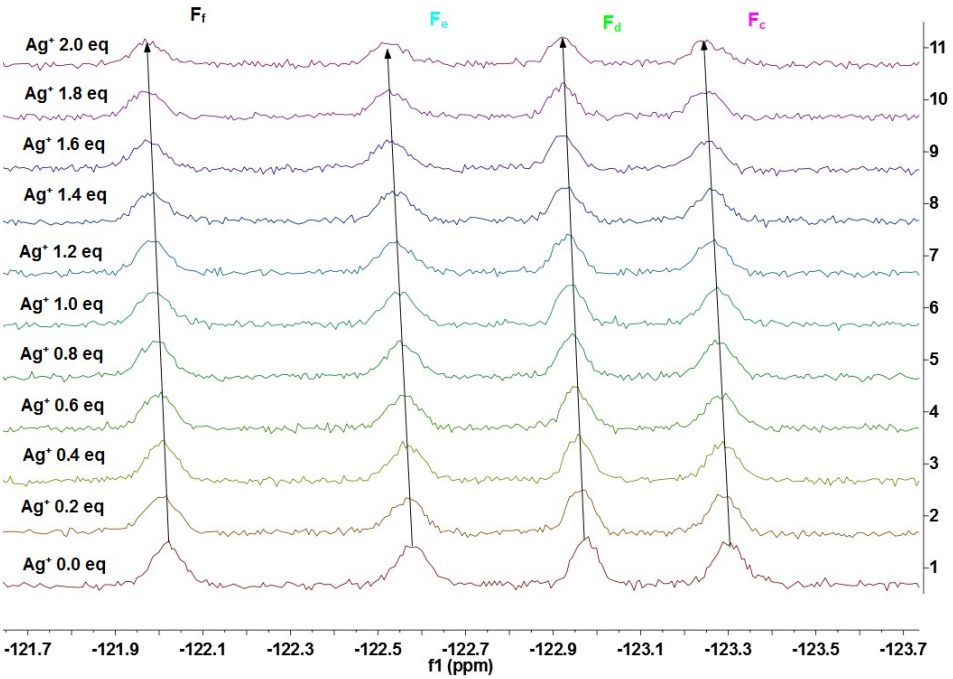

Fig. S9 Partial ^{19}F NMR spectra of F_c, F_d, F_e and F_f of L-**1** in the presence of Ag^+ in EtOD. [L-**1**] = 50 μM.

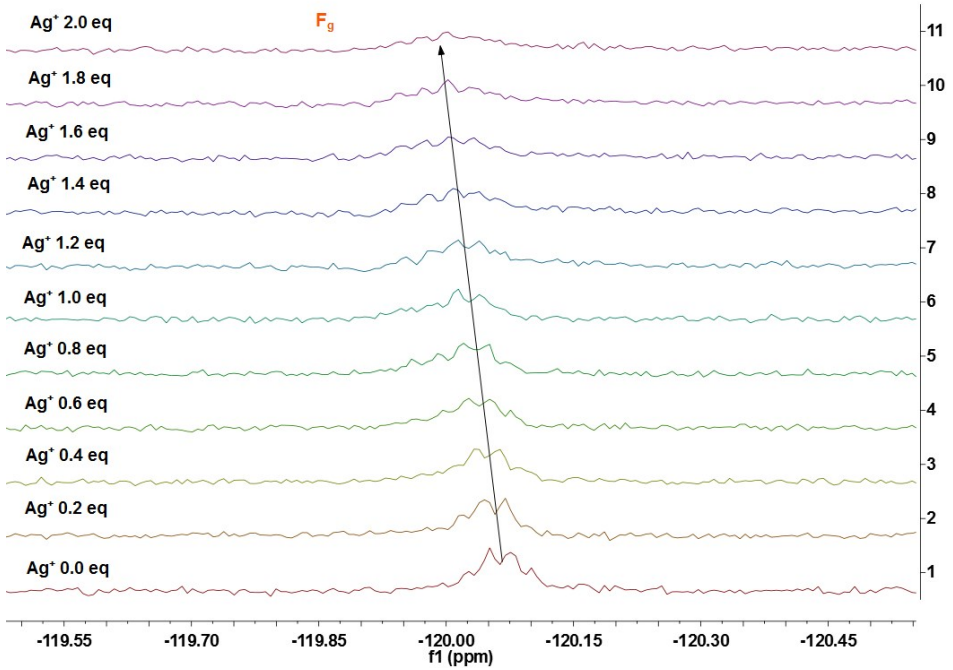

Fig. S10 Partial ^{19}F NMR spectra of F_g of L-**1** in the presence of Ag^+ in EtOD. [L-**1**] = 50 μM.

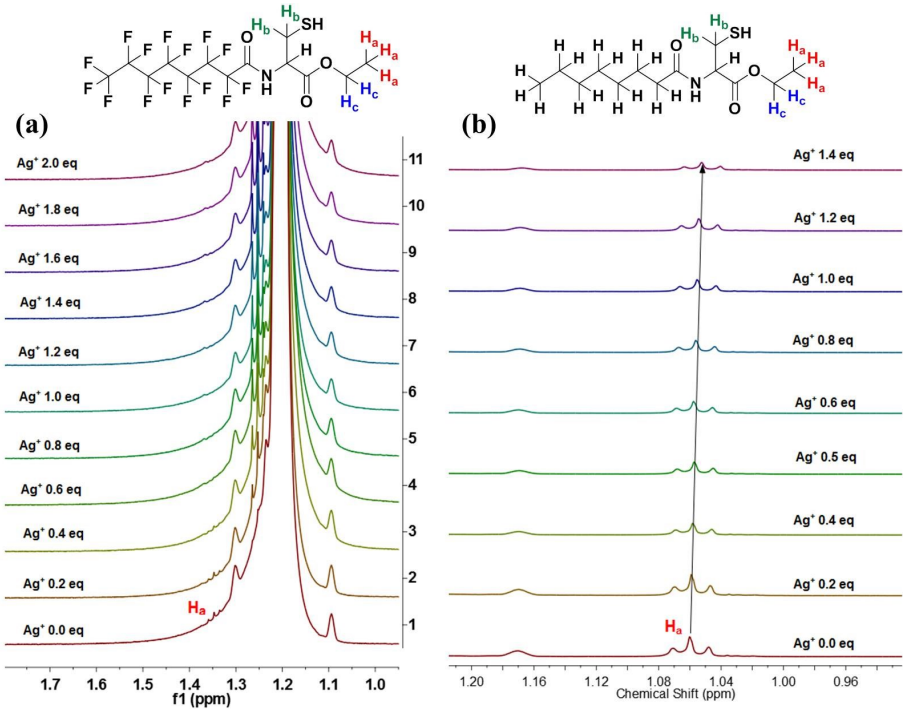

Fig. S11 Partial ^{1}H NMR spectra of H_a of L-**1** (a) and L-**2** (b) in the presence of Ag^{+} in EtOD. [L-**1**] = [L-**2**] = 50 μM.

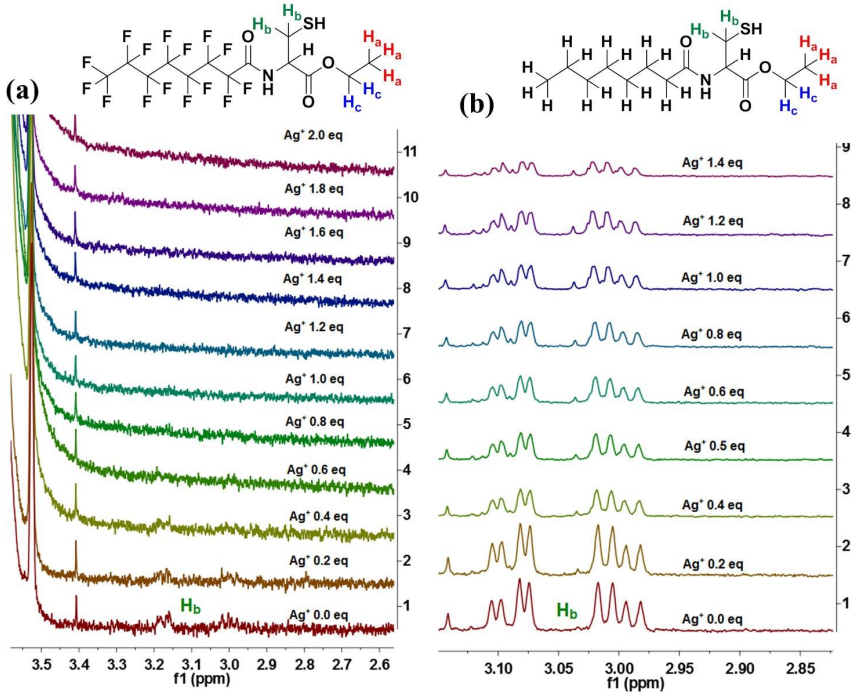

Fig. S12 Partial ^{1}H NMR spectra of H_b of L-**1** (a) and L-**2** (b) in the presence of Ag^{+} in EtOD. [L-**1**] = [L-**2**] = 50 μM.

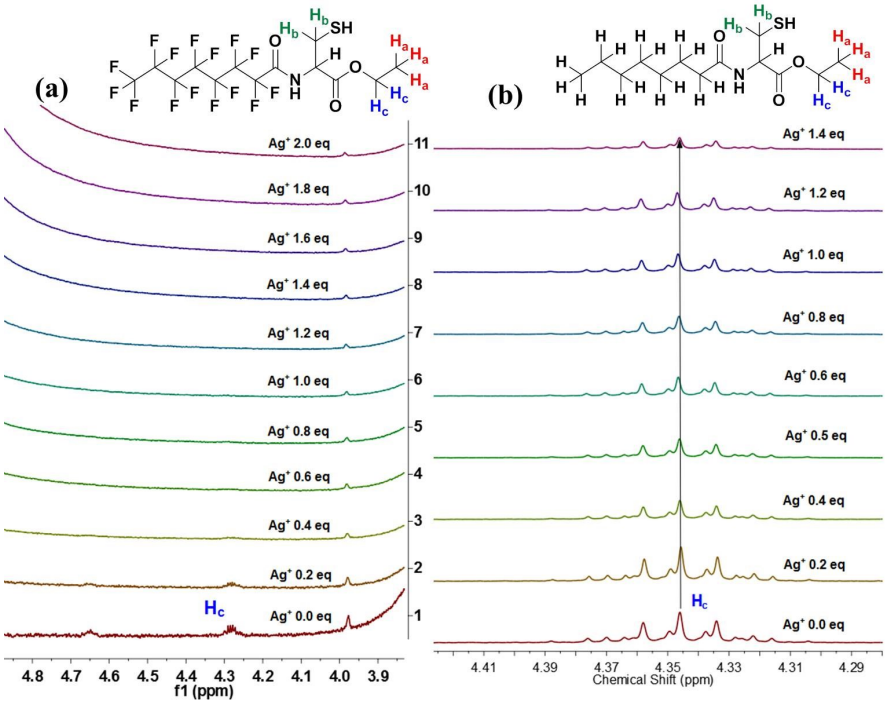

Fig. S13 Partial ^{1}H NMR spectra of H_c of L-**1** (a) and L-**2** (b) in the presence of Ag^+ in EtOD. [L-**1**] = [L-**2**] = 50 μM.

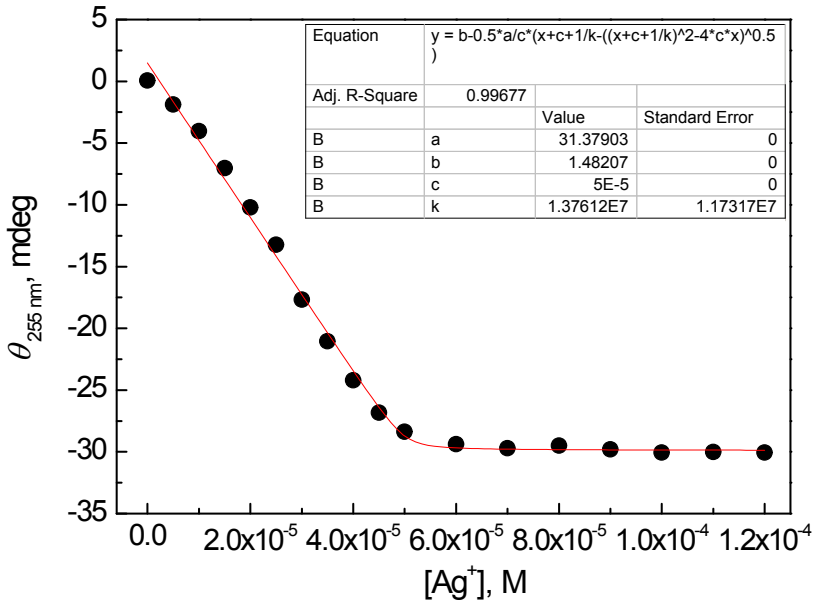

Fig. S14 Data fitting of CD signal at 255 nm of Ag^+-L-**1** in EtOH as a function of concentration of Ag^+ assuming a 1:1 stoichiometry. [L-**1**] = 50 μM, [Ag^+] = 0 - 120 μM.

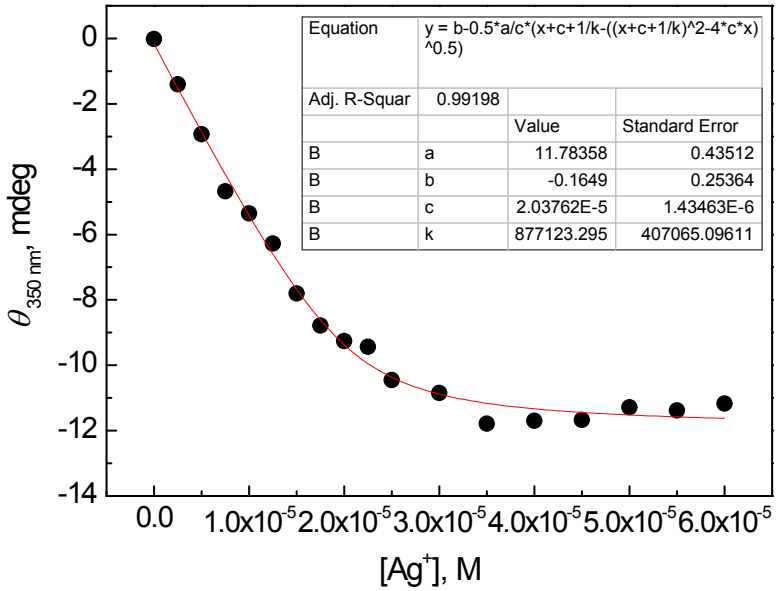

Fig. S15 Data fitting of CD signal at 350 nm of Ag^+-L-**2** in EtOH as a function of concentration of Ag^+ assuming a 1:1 stoichiometry. [L-**2**] = 25 μM, [Ag^+] = 0 - 60 μM.

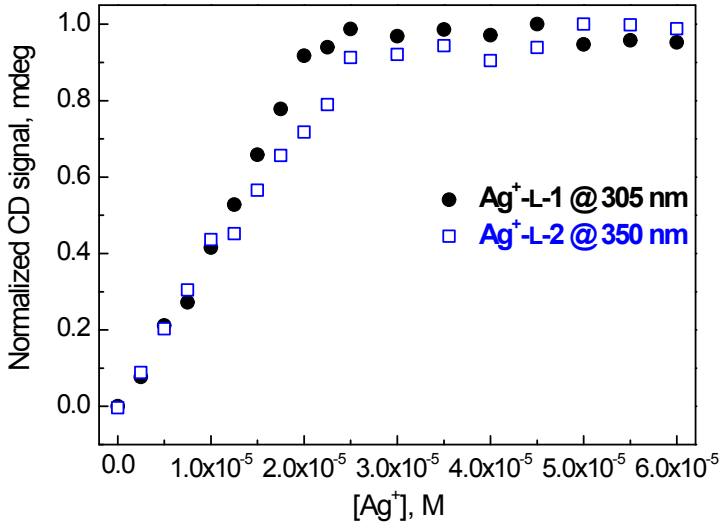

Fig. S16 Normalized CD signals at 305 nm of Ag^+-L-**1** and 350 nm of Ag^+-L-**2** in EtOH with increasing concentration of Ag^+. [L-**1**] = [L-**2**] = 25 μM, [Ag^+] = 0 - 60 μM.

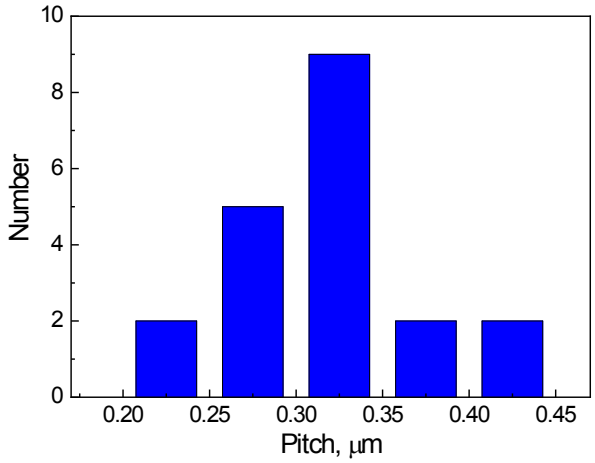

Fig. S17 Histogram of the helical pitch of structure observed in the SEM images from the Ag^{+}-L-**1** complex in EtOH. [L-**1**] = [Ag^{+}] = 25 μM.

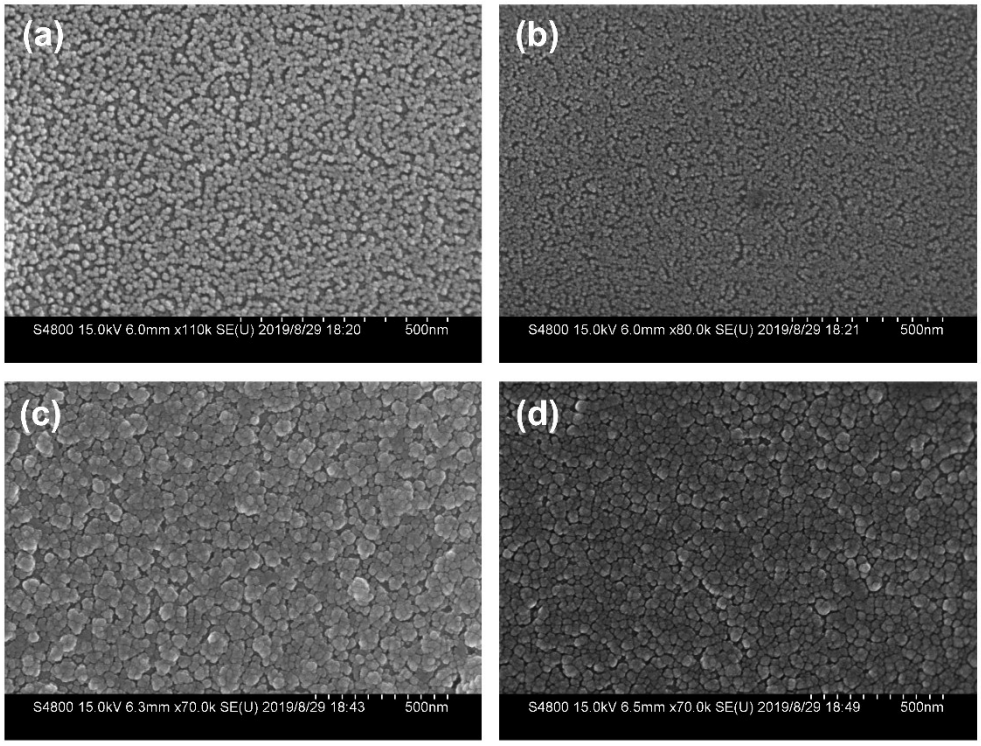

Fig. S18 SEM images of the structures of L-**1** (a), D-**1** (b) and L-**2** (c), D-**2** (d) formed in EtOH. [L-**1**] = [D-**1**] = [L-**2**] = [D-**2**] = 25 μM.

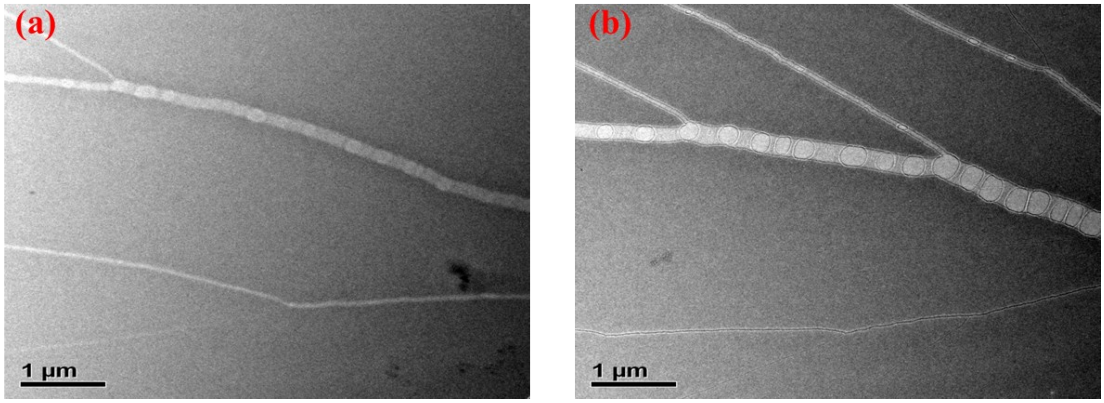

Fig. S19 TEM images of supramolecular structures formed in EtOH solutions of Ag^+-L-**1** (a) and Ag^+-D-**1** (b).

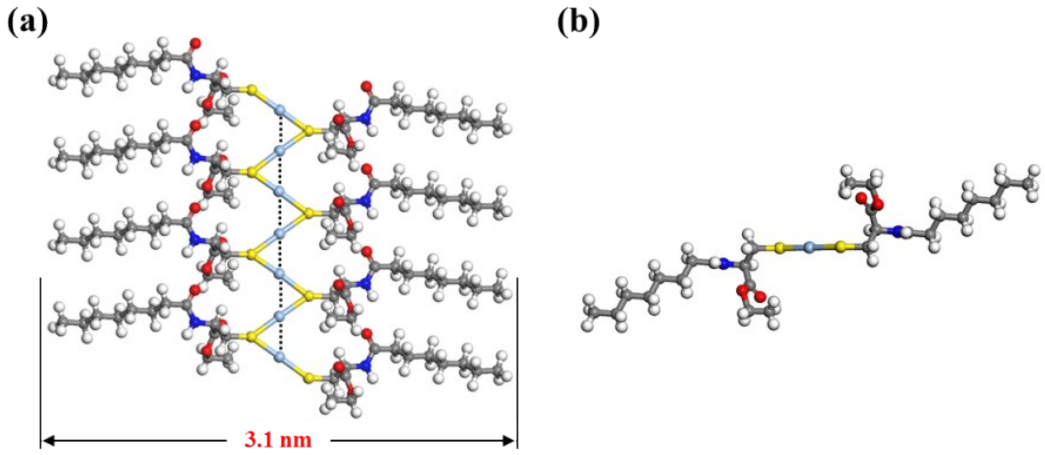

Fig. S20 Structural models of Ag^+-**2** polymeric chain from the front view (a) and the side view (b) using Materials Studio modeling. Dashed black lines highlight the $Ag^+\cdots Ag^+$ interactions.

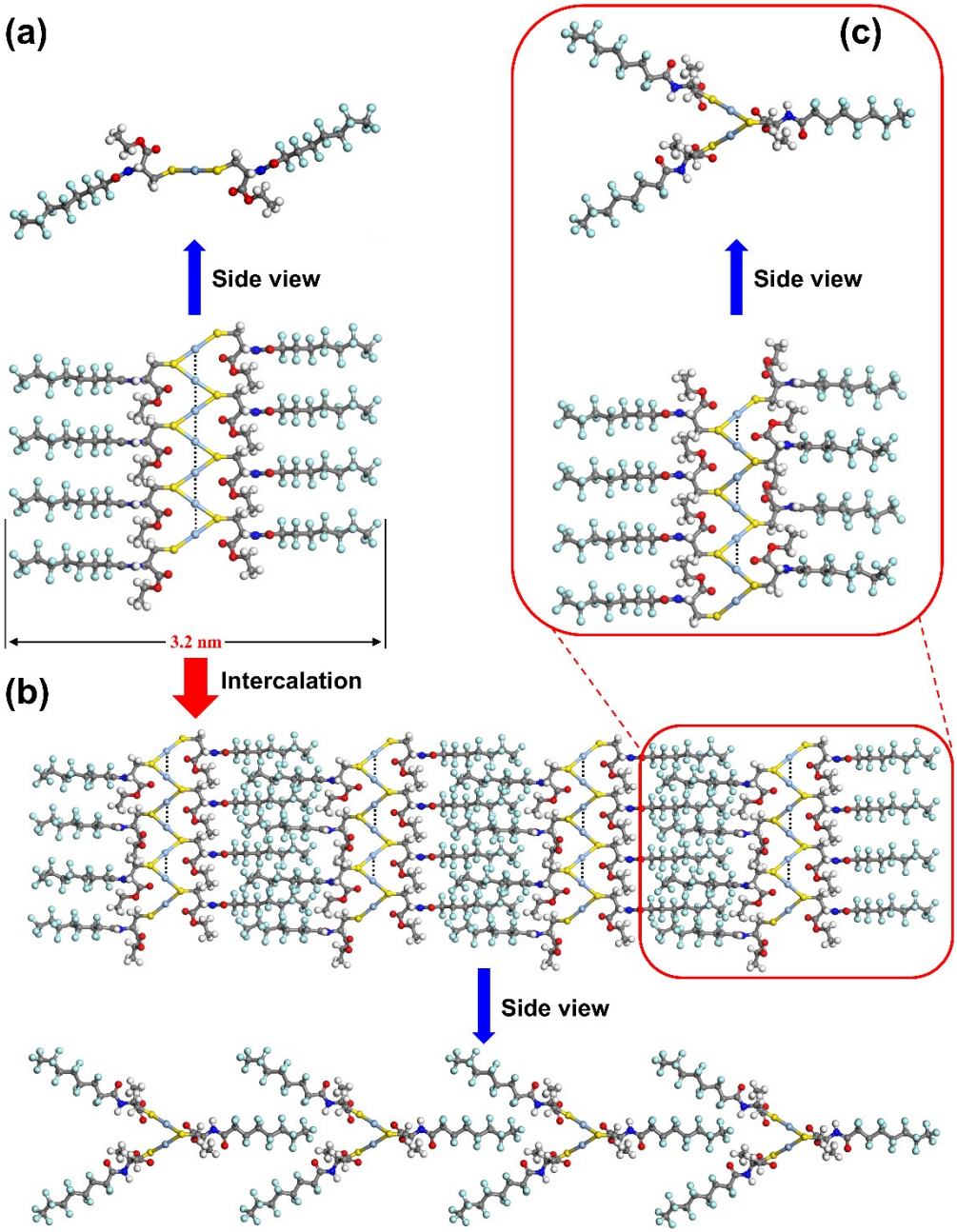

Fig. S21 (a) Structural models of single Ag^{+}-**1** polymeric chain. (b) Structural models of the inter-chain intercalation between Ag^{+}-**1** polymeric chains. (c) Single Ag^{+}-**1** polymeric chain extracted from the intercalation. Dashed black lines highlight the $Ag^{+}\cdots Ag^{+}$ interactions. The structural models are shown by using Materials Studio modeling. The extended $Ag^{+}\cdots Ag^{+}$ interactions in single polymeric chain (a) turn to the binuclear $Ag^{+}\cdots Ag^{+}$ interactions due to inter-chain intercalation (c).

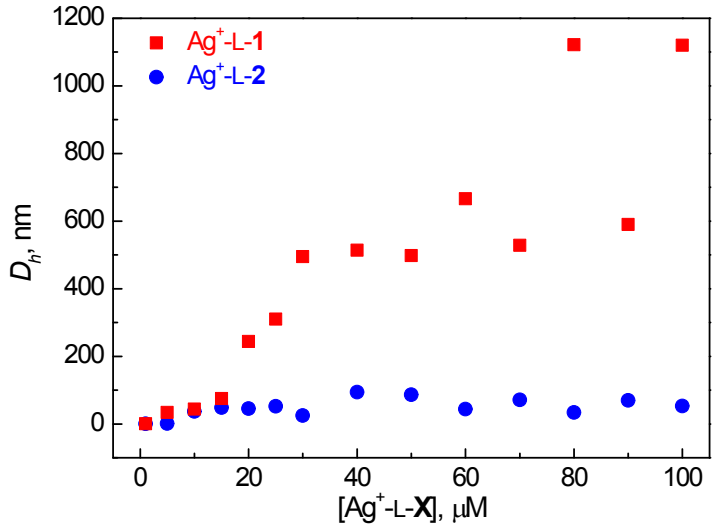

Fig. S22 Hydrodynamic diameters of Ag^+-L-**1** and Ag^+-L-**2** in EtOH in the presence of Ag^+ of increasing concentration. [L-**1**] = [L-**2**] = [Ag^+].

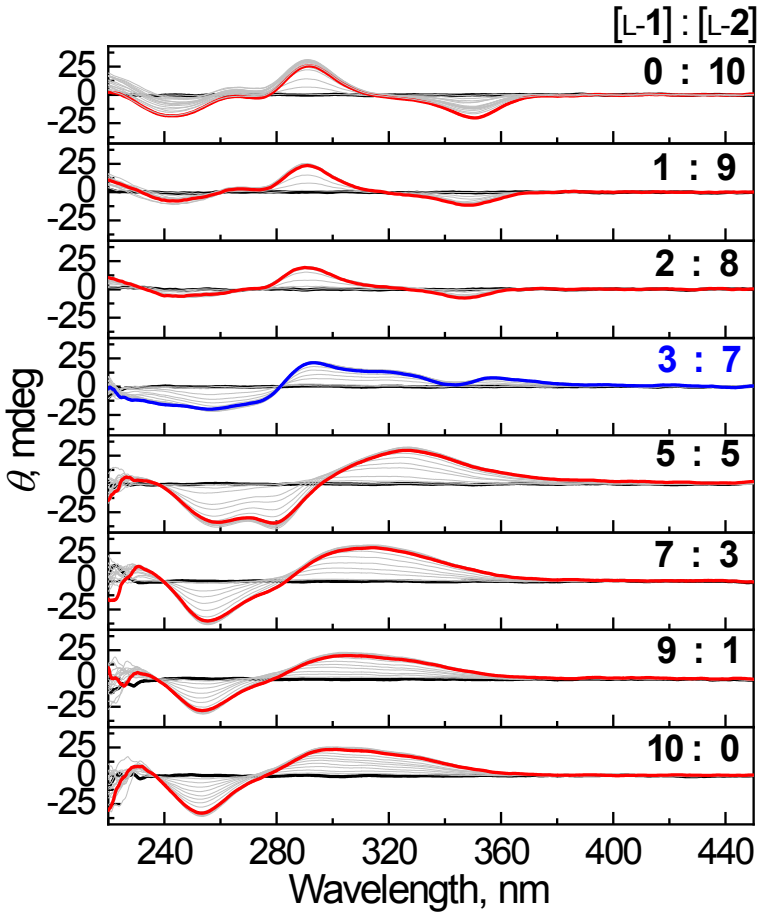

Fig. S23 CD spectra of L-**1** and L-**2** of varying molar ratio in EtOH in the presence of Ag^+ of increasing concentration. [L-**1**] + [L-**2**] = 25 μM, [Ag^+] = 0 - 60 μM.

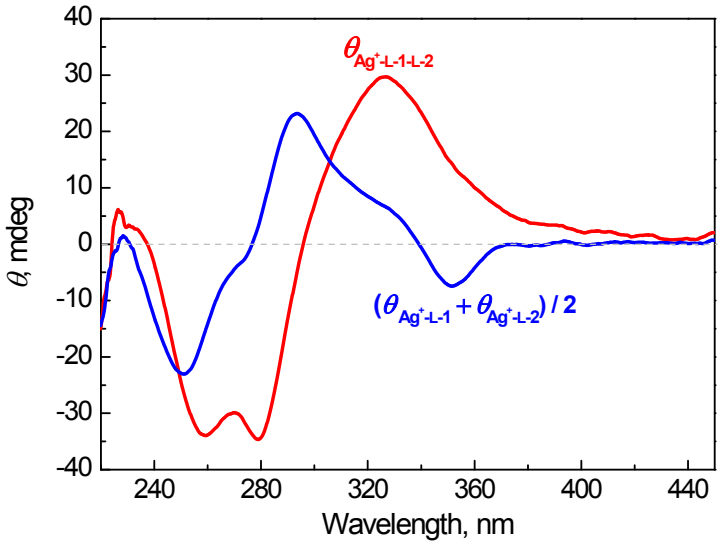

Fig. S24 Calculated (blue line) and experimental (red line) CD spectra of Ag^+-L-**1**-L-**2** (molar ratio of L-**1** to L-**2** is 5:5) in EtOH. Calculated line is from individual CD spectra of Ag^+-L-**1** and Ag^+-L-**2** according to $\theta_{calcd.} = (\theta_{Ag^+\text{-L-}\mathbf{1}} + \theta_{Ag^+\text{-L-}\mathbf{2}})/\mathbf{2}$. [L-**1**] + [L-**2**] = [Ag^+] = 25 μM.

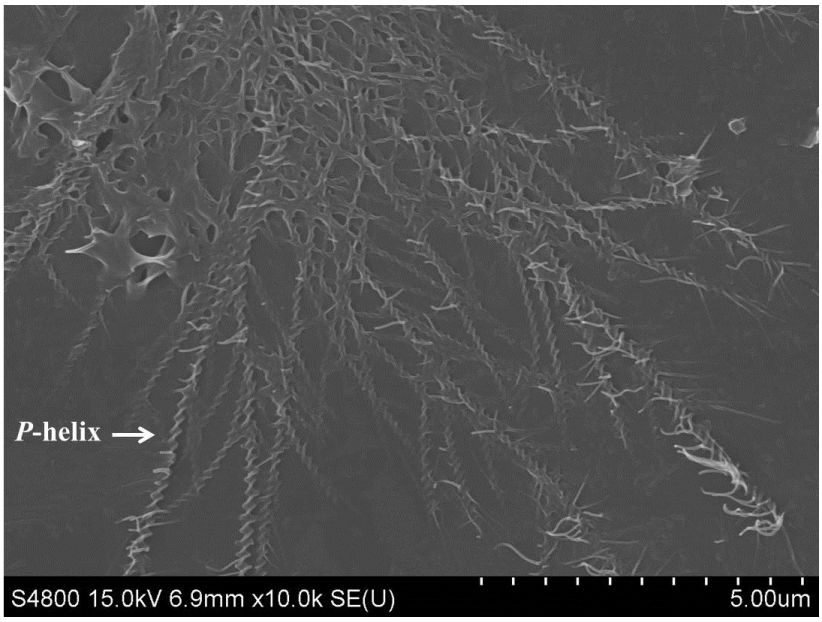

Fig. S25 SEM image of the mixed ligands of L-**1** and L-**2** of molar ratio 5:5 in EtOH in the presence of Ag^+. [L-**1**] + [L-**2**] = [Ag^+] = 25 μM.

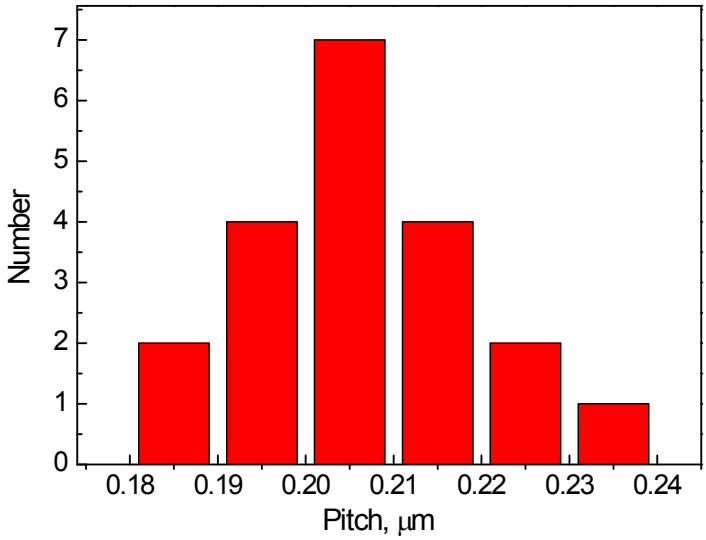

Fig. S26 Helical pitch of structures observed from Ag^+-L-**1**-L-**2** at L-**1** to L-**2** molar ratio of 5:5 in EtOH. [L-**1**] + [L-**2**] = [Ag^+] = 25 μM.

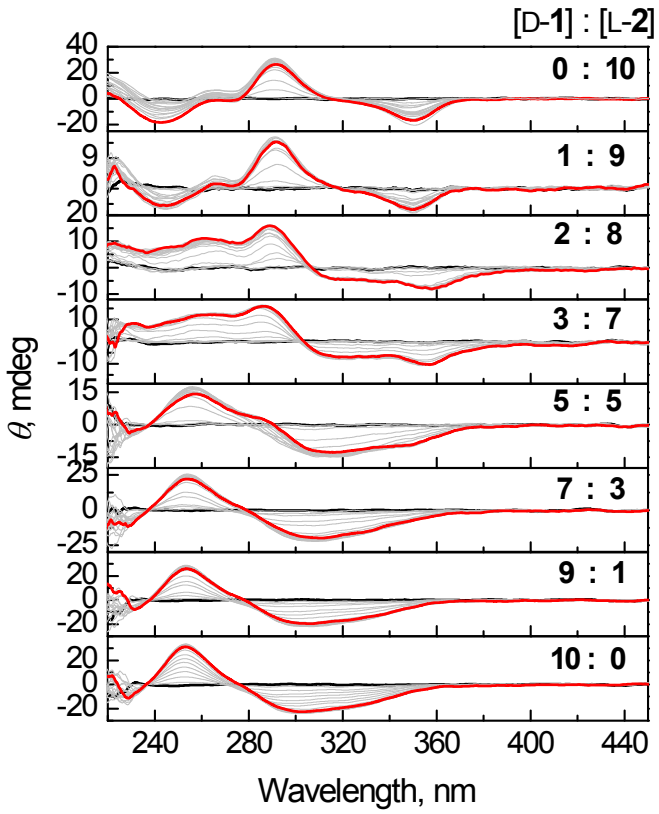

Fig. S27 CD spectra of the mixed ligands of D-**1** and L-**2** of different molar ratio in EtOH in the presence of Ag^+. [D-**1**] + [L-**2**] = 25 μM, [Ag^+] = 0 - 60 μM.

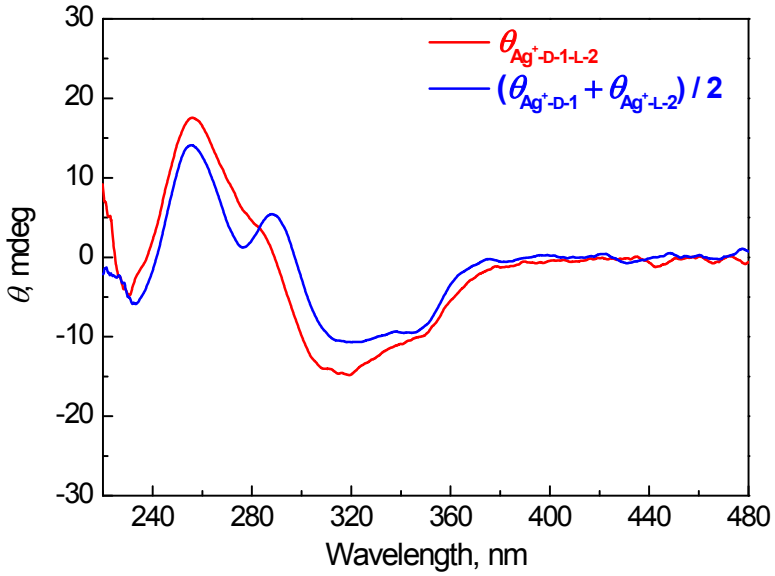

Fig. S28 Calculated (blue line) and experimental (red line) CD spectra of Ag^+-D-**1**-L-**2** (molar ratio of D-**1** to L-**2** is 5:5) in EtOH. Calculated line is from the individual CD spectra of Ag^+-D-**1** and Ag^+-L-**2** according to $\theta_{calcd.} = (\theta_{Ag+\text{-}D\text{-}1} + \theta_{Ag+\text{-}L\text{-}2})/2$. [D-**1**] + [L-**2**] = [Ag^+] = 25 μM.

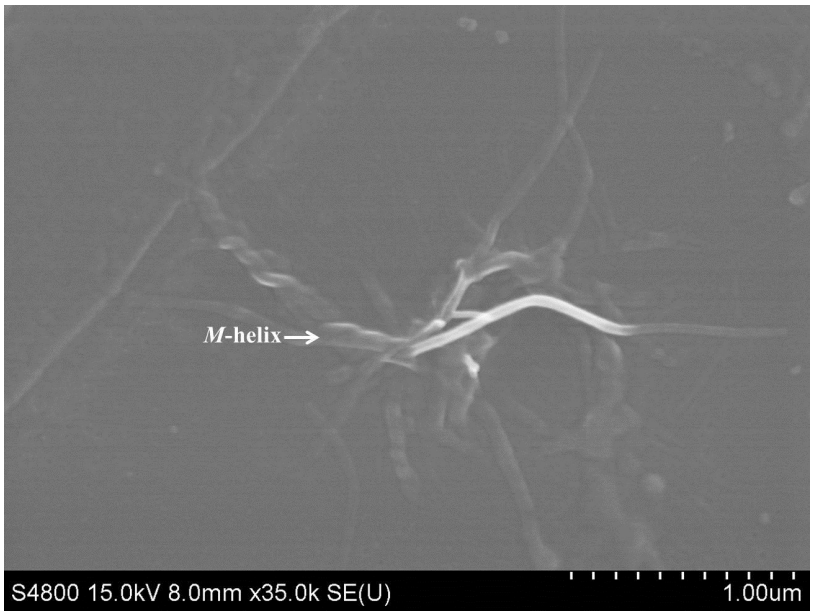

Fig. S29 SEM image of the mixed ligands of D-**1** and L-**2** at molar ratio of 5:5 in EtOH in the presence of Ag^+. [D-**1**] + [L-**2**] = [Ag^+] = 25 μM.

S2.2 ^{1}H NMR, ^{13}C NMR, and ^{19}F NMR spectra of 1 and 2

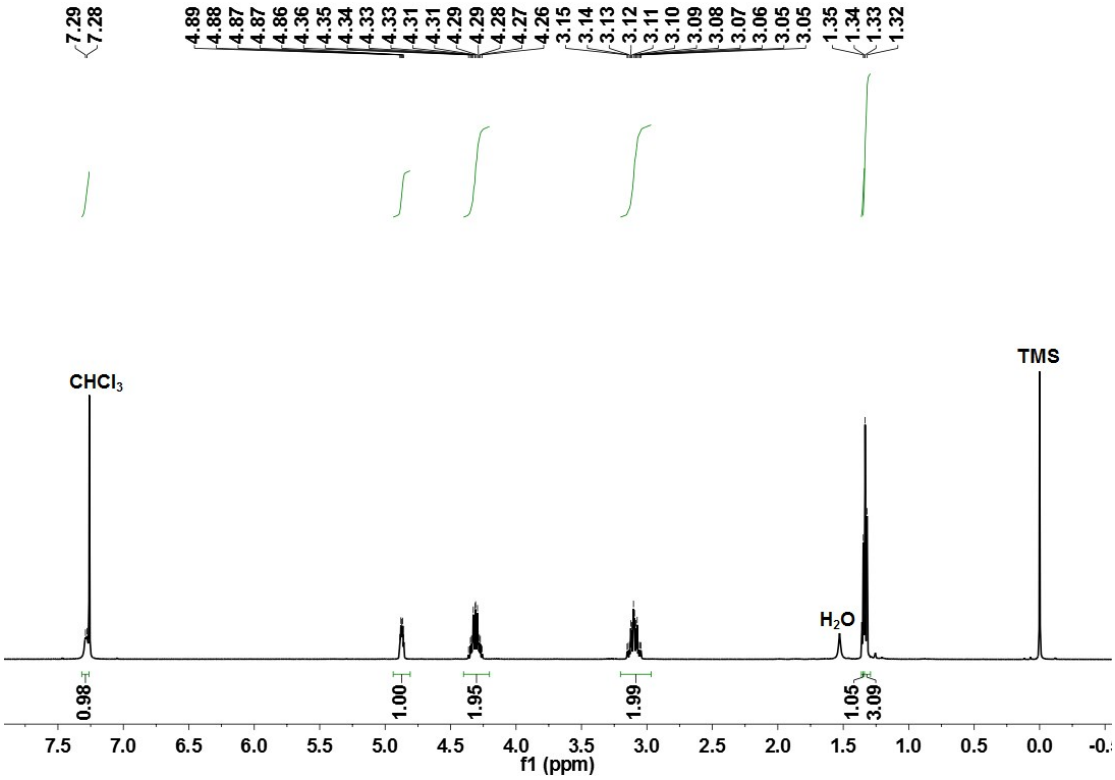

Fig. S30 ^{1}H NMR of L-**1** (500 MHz, $CDCl_3$)

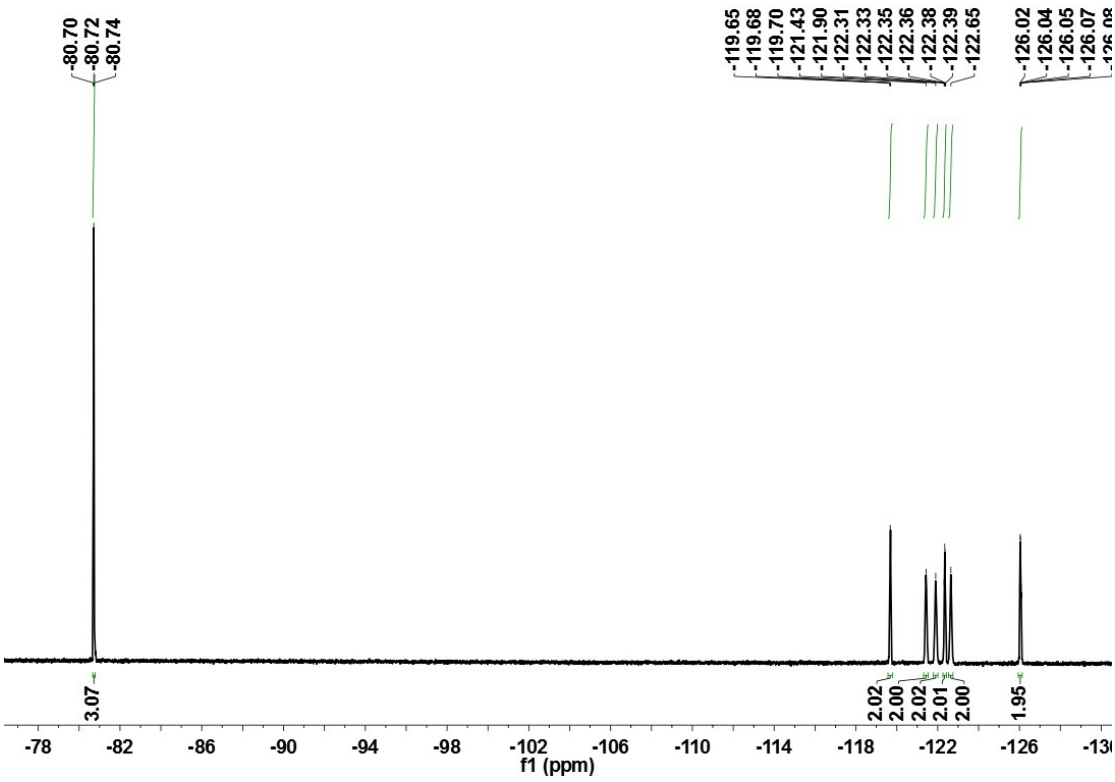

Fig. S31 ^{19}F NMR of L-**1** (600 MHz, $CDCl_3$)

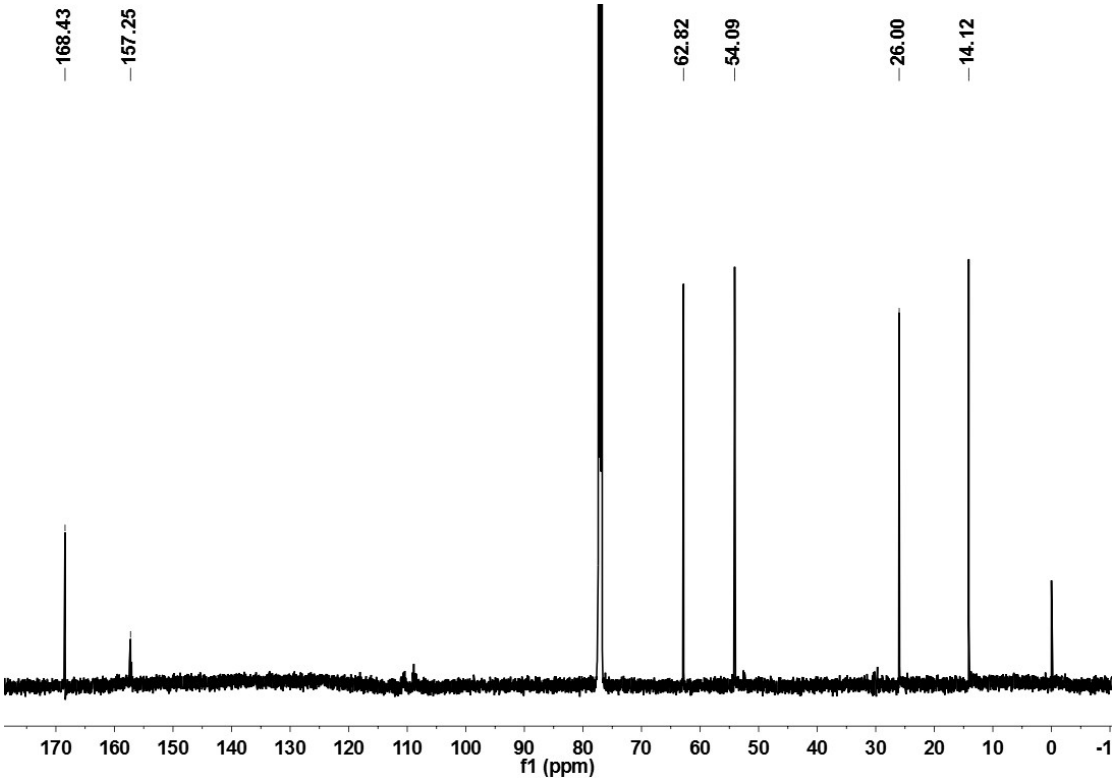

Fig. S32 ^{13}C NMR of L-**1** (126 MHz, $CDCl_3$)

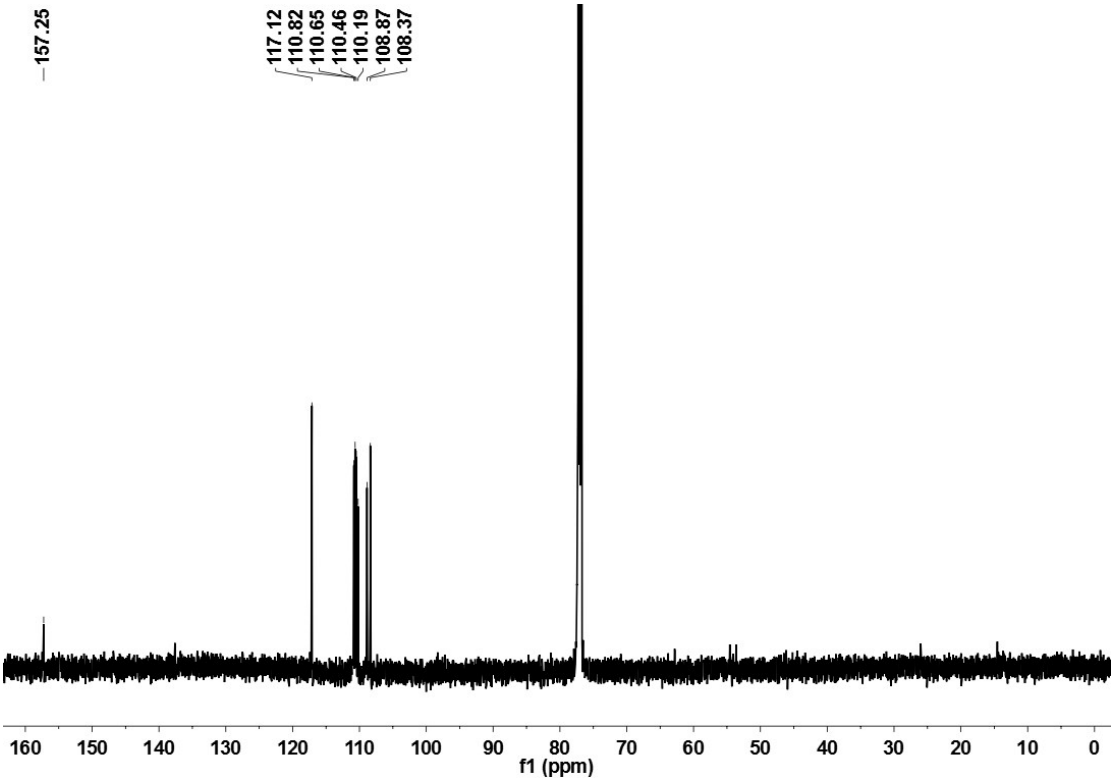

Fig. S33 ^{13}C NMR of L-**1** (126 MHz, $CDCl_3$)

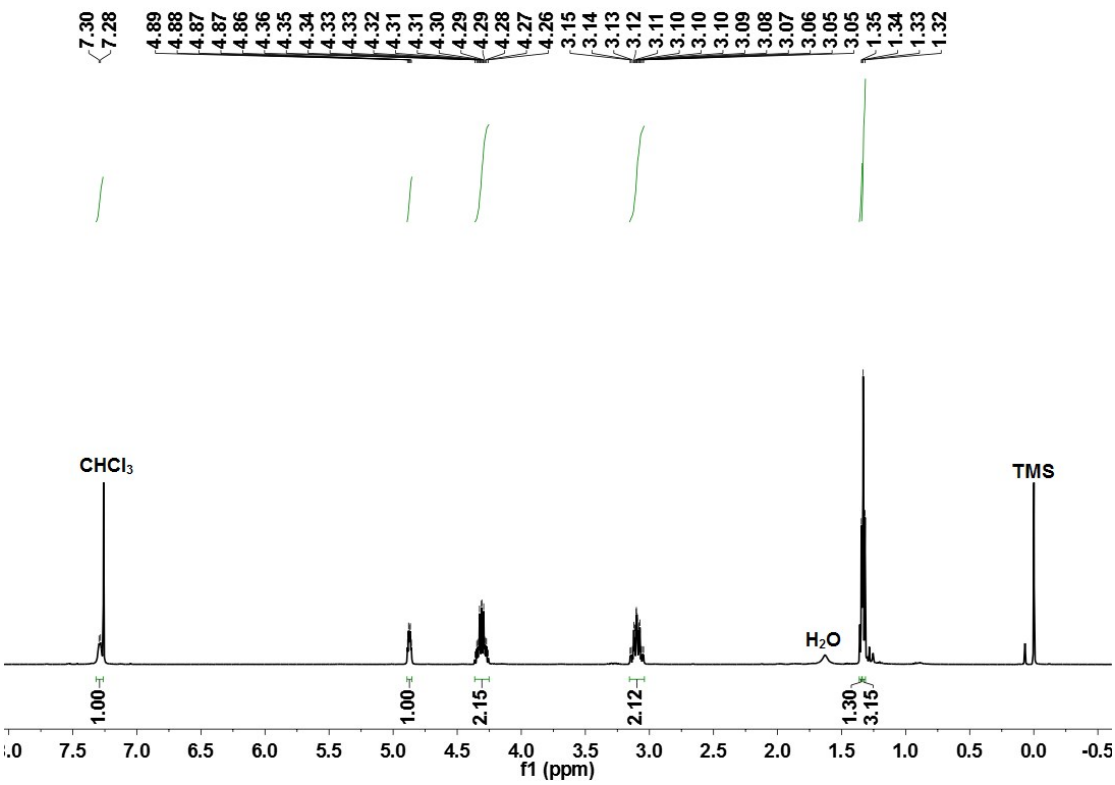

Fig. S34 ^{1}H NMR of D-**1** (500 MHz, $CDCl_3$)

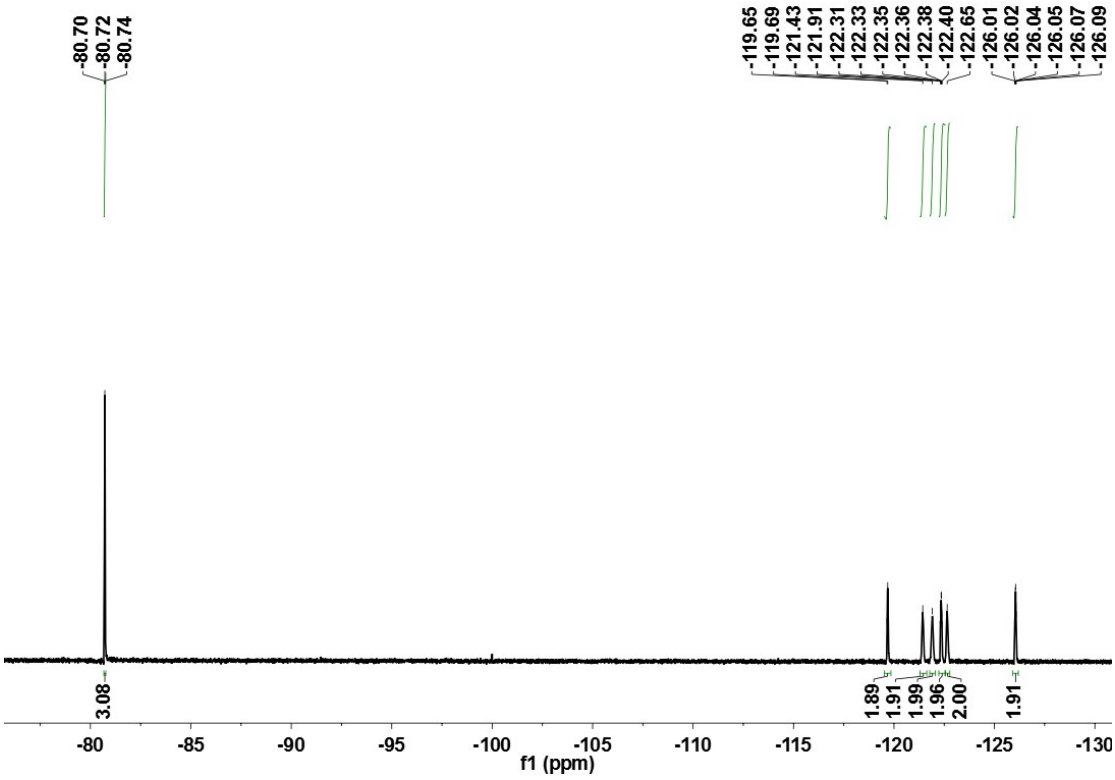

Fig. S35 ^{19}F NMR of D-**1** (600 MHz, $CDCl_3$)

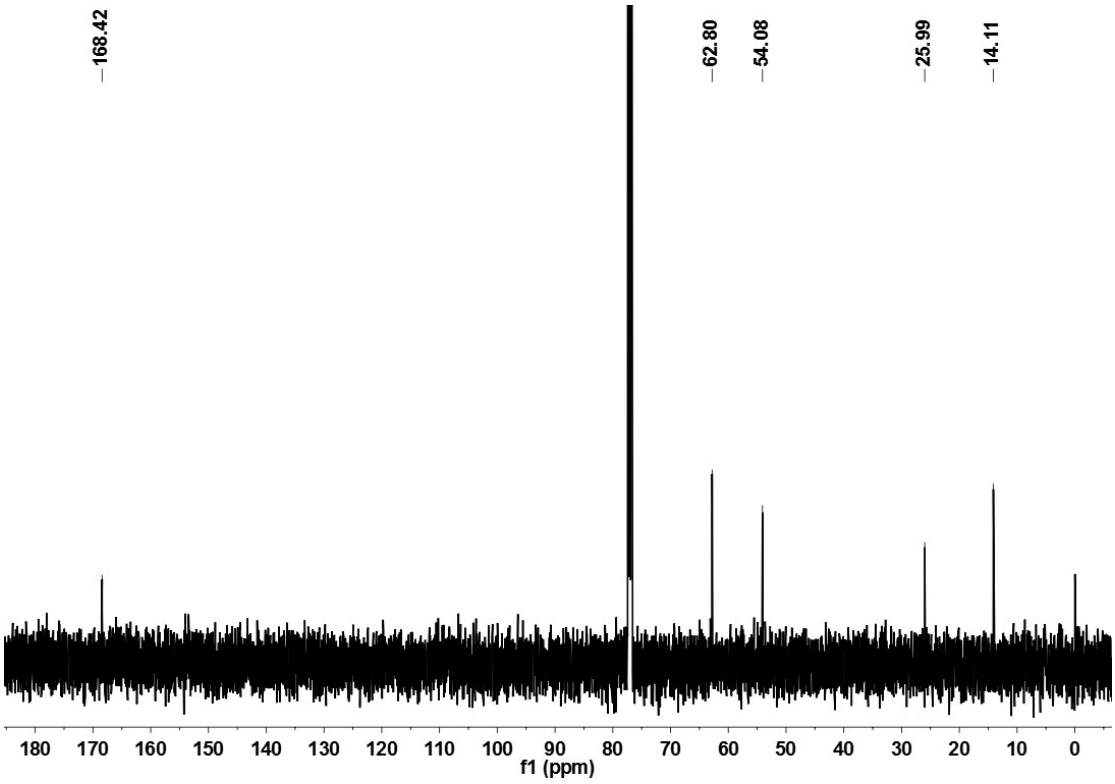

Fig. S36 ^{13}C NMR of D-**1** (126 MHz, $CDCl_3$)

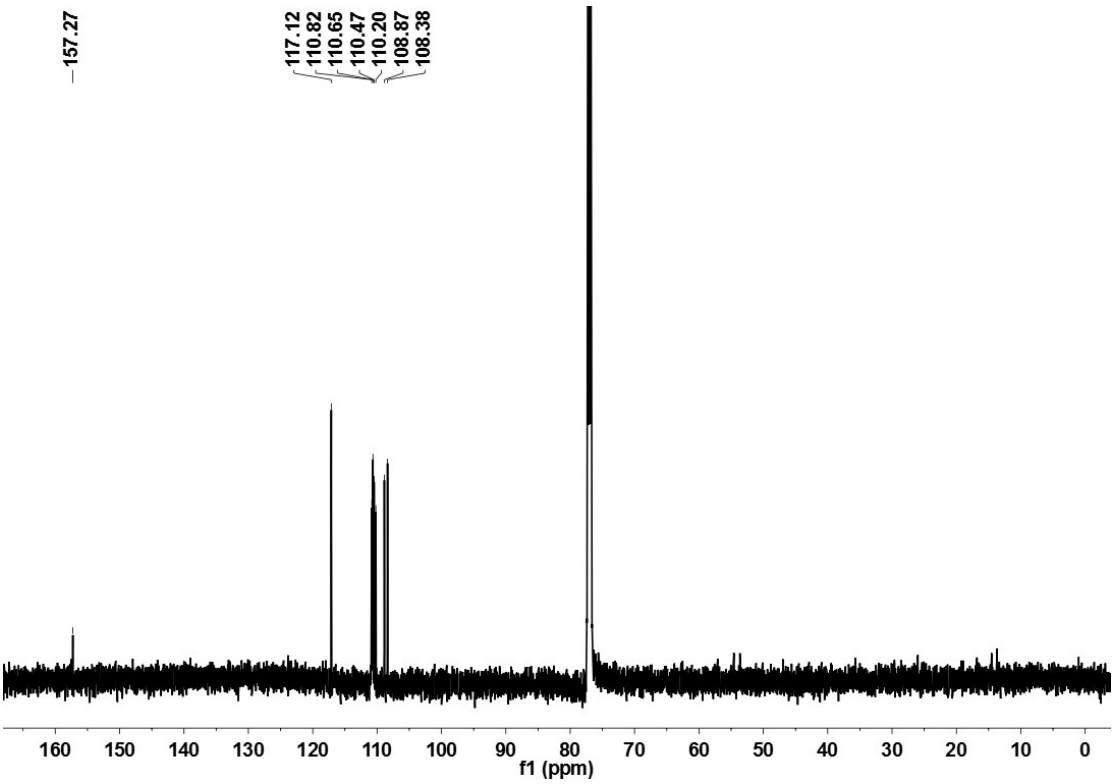

Fig. S37 ^{13}C NMR of D-**1** (126 MHz, $CDCl_3$)

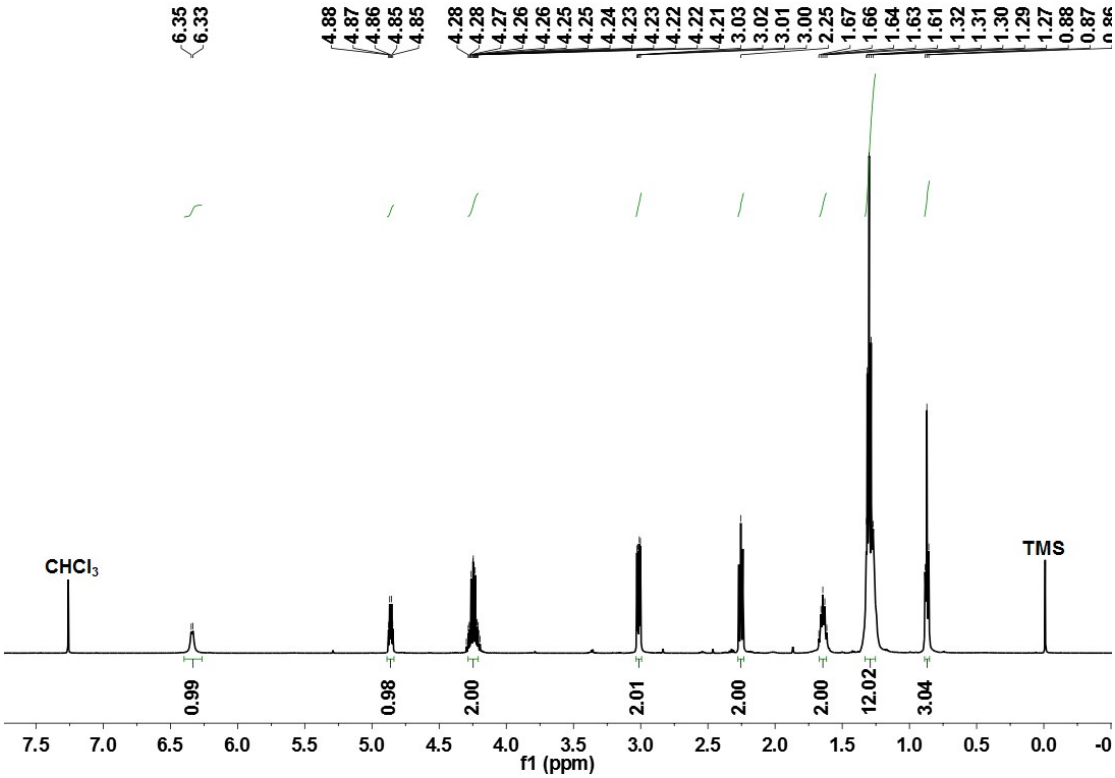

Fig. S38 ^{1}H NMR of L-**2** (500 MHz, $CDCl_3$)

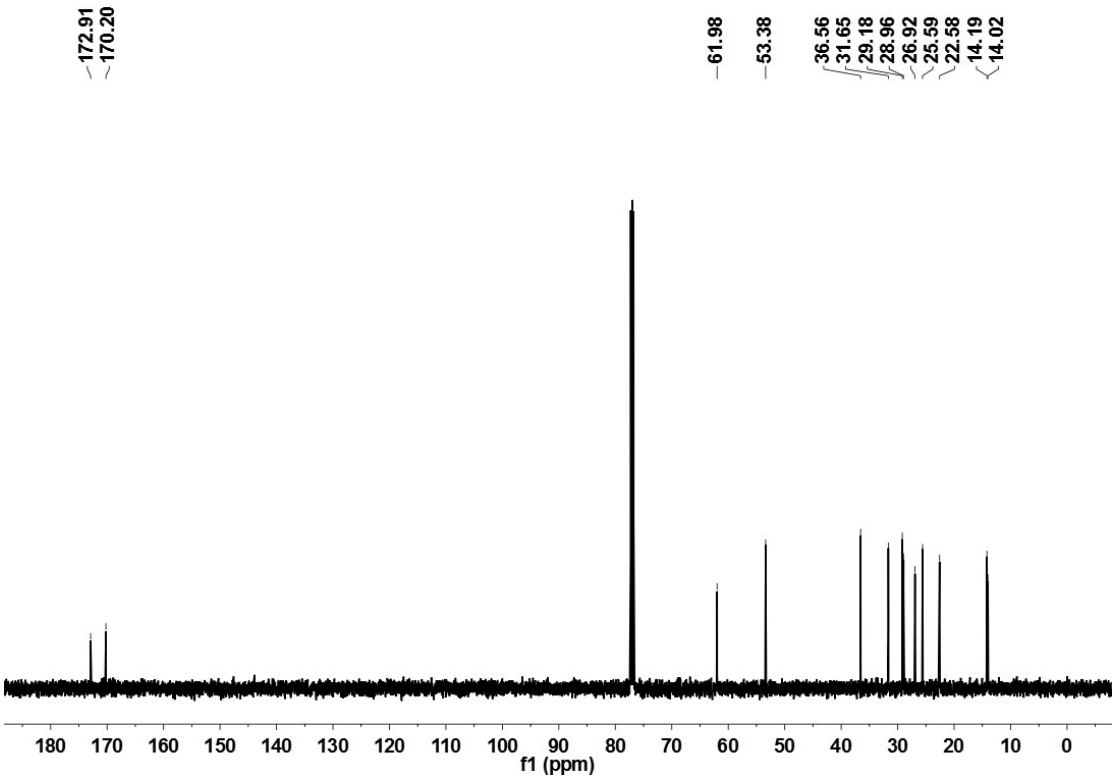

Fig. S39 ^{13}C NMR of L-**2** (126 MHz, $CDCl_3$)

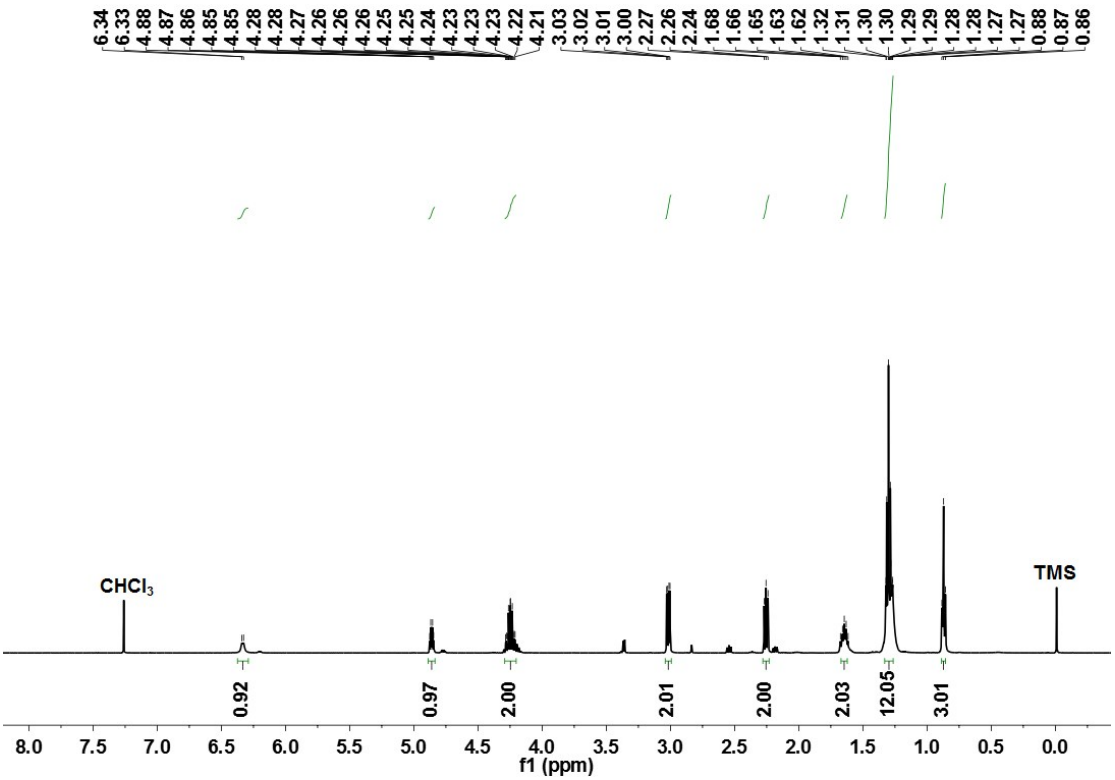

Fig. S40 ^{1}H NMR of D-**2** (500 MHz, $CDCl_3$)

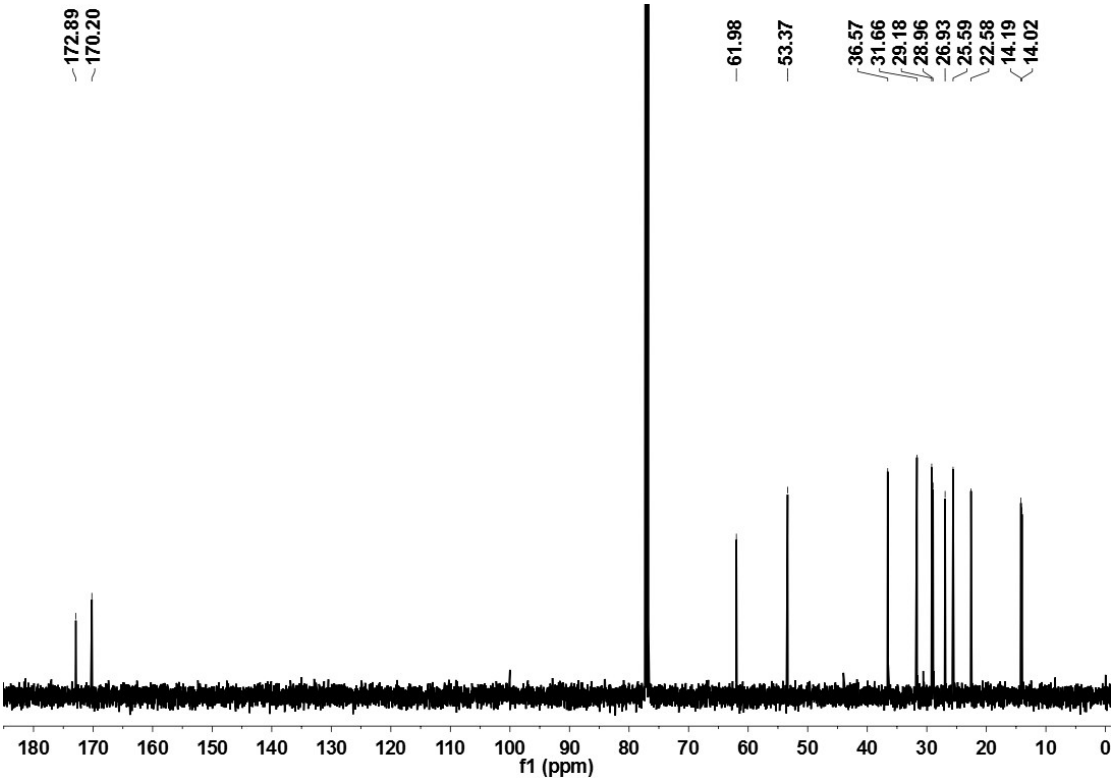

Fig. S41 ^{13}C NMR of D-**2** (126 MHz, $CDCl_3$)